We are IntechOpen, the world's leading publisher of Open Access books Built by scientists, for scientists

4,800
Open access books available

122,000
International authors and editors

135M
Downloads

Our authors are among the

154
Countries delivered to

TOP 1%
most cited scientists

12.2%
Contributors from top 500 universities

WEB OF SCIENCE™

Selection of our books indexed in the Book Citation Index in Web of Science™ Core Collection (BKCI)

Interested in publishing with us?
Contact book.department@intechopen.com

Numbers displayed above are based on latest data collected.
For more information visit www.intechopen.com

Chapter 15

Surface Acoustic Wave Based Magnetic Sensors

Bodong Li, Hommood Al Rowais and Jürgen Kosel

Additional information is available at the end of the chapter

http://dx.doi.org/10.5772/55220

1. Introduction

Since the radar system was invented in 1922, the development of devices communicating by means of reflected power has experienced a continuously growing interest. In 1948, Harry Stockman published a paper [1] in which he laid the basis for the idea of radio frequency identification (RFID), and the first patent had been filed in 1973 by Charles Walton. After decades of research and commercialization, RFID products became a part of everyday life (e.g. logistics, access control, security). With the growing interest in remote and battery-free devices, researchers are pushing the boundaries of RFID technology to find solutions in new fields like sensing applications.

For many sensors such as those operated in remote or harsh environments, the sensitivity is not the only evaluation criteria. The lifetime, especially of the power source, and the complexity added by wiring often demand wireless and passive operation. Batteries have limited lifetime and also add to the size and mass of the sensors. Alternatively, energy harvesting or an RF-based wireless power supply can be employed [2, 3]. The former method depends on environmental conditions such as solar radiation, temperature change, chemical reagents, vibration etc., which are often not constantly or not sufficiently available. RF power sources, on the other hand, transmit power wirelessly and with full control over amount and timing.

Passive and remote sensors utilizing SAW transponders are devices, which are powered by an RF source. These systems require an interrogation device that requests the sensor signal, a SAW transponder plus a sensing element and two antennas. The basic idea is that an RF signal of certain frequencies generated by the interrogator is received by the SAW transponder, which reflects back a signal modified by the sensing element. This signal contains the environmental information in an amplitude and phase change, which is converted into the physical parameters by the interrogator. In most cases, SAW sensors are coded by having different reflector designs in order to have multiple measurement capabilities from sensors located in the same interrogation area. A great amount of research

has been carried out in the past decades in this field, and, as a result, different wireless SAW sensors have been developed to measure a variety of physical and chemical parameters including temperature, stress, torque, pressure, humidity, magnetic field, chemical vapor etc. [4-9]. Several devices are already commercialized [10-12].

SAW-based magnetic sensors have, so far, not been studied in detail. Magnetic sensors are one of the most pervasive kinds of sensors for a large number of applications and are employed in different fields like automotive, biomedical or consumer electronics. Integrating magnetic sensors with SAW transponders enables remote and passive operation, thereby, opens a door for further applications. Early in 1975, a magnetically tuned SAW phase shifter was proposed by Ganguly et al [13]. A thin film of magnetostrictive material was fabricated on the delay line of a SAW device. A phase shift was observed due to the dependence of the wave propagation velocity on the external magnetic field. Recently, a new concept of a magnetic sensor based on a SAW resonator has been published [8]. A magnetostrictive material was used to fabricate the interdigital transducers (IDT) of the SAW device. The resonant frequency of the device changes with an external magnetic field. A different idea was put forth by Hauser and Steindl [14-16] combining a SAW transducer with a giant magnetoimpedance (GMI) microwire sensor. The GMI sensor has a magnetic sensitivity, at least, one order higher than contemporary giant magnetoresistance (GMR) sensors and can be used to measure very low magnetic fields such as those generated by the human heart or muscles. A GMI sensor is operated by an ac current and the impedance changes upon changes of a magnetic field. This makes it a suitable load for a SAW transponder, which converts this impedance change into a magnitude and phase change of the reflected acoustic waves. In order to reduce the size and improve the level of integration of the senor, a new design of an integrated SAW transponder and thin film GMI sensor has been proposed and developed recently by the authors [17, 18]. The SAW transponder and GMI thin film were integrated on the same chip using standard micro-fabrication technology suitable for mass fabrication.

The ideal SAW-based magnetic sensor is small and highly integrated, inexpensive, passive, remotely controlled and have a high magnetic sensitivity together with a large linear range. With regard to these criterions, an SAW-GMI sensor is a very promising candidate.

SAW-based magnetic sensors have been studied for several years. However, this topic has yet not been comprehensively summarized, and the aim of this chapter is to provide a systematic review of the past research as well as the latest results. The performance of the devices crucially depends on different design parameters in a complex fashion. This will be shown by a detailed description and analysis for a device consisting of a SAW transponder and GMI thin film sensor.

2. SAW based passive sensors

A basic SAW device consists of an input interdigital transducer (IDT) and an output (or reflector) IDT, which are fabricated on a piezoelectric substrate. The area between the input IDT and output IDT is called the delay line. The IDT is made of two metallic, comb-like

structures arranged in an interdigital fashion, whereby the distance between two fingers of a comb defines the periodicity (p) (Fig. 1). Upon application of a voltage, charges accumulate at the fingers of the IDT depending on the capacitance of the structure. The resulting electric field generates stress in the substrate due to the piezoelectric effect. If an ac input voltage is applied, the continuously changing polarity of the charges will excite an SAW (Rayleigh wave) traveling through the substrate. At the operating (resonant) frequency of the SAW device, the value of p equals the wavelength of the SAW, and the SAW amplitude shows a maximum value due to constructive superposition.

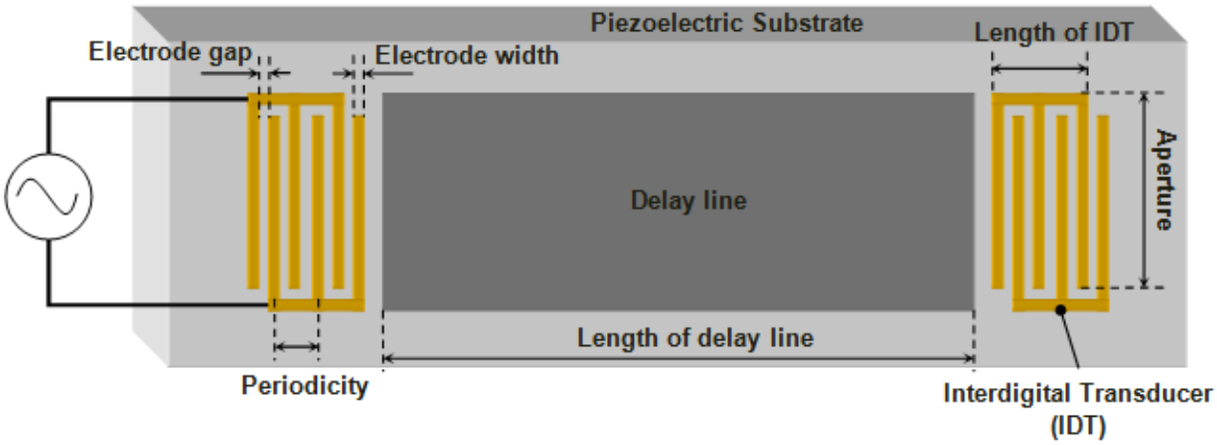

Figure 1. Schematic of a SAW device.

2.1. Basics of SAW devices

SAW Resonant Frequency: The resonant motion of an acoustic resonator is caused by the coupling between the transducer (IDT) and the acoustic medium. The resonant frequency, or operating frequency, is determined by the periodicity and the acoustic wave velocity (v)

$$f = \frac{v}{p}. \tag{1}$$

The value of v mainly depends on the substrate's material. A typical SAW velocity for piezoelectric materials is several thousand meters per second. Due to the intrinsic anisotropy of piezoelectric materials, v is dependent on the direction of propagation. Since different acoustic modes have different wave velocities, a device can resonate at different frequencies. The SAWs are Rayleigh waves, which have a longitudinal and a vertical shear component that can couple with any media in contact with the surface. This coupling strongly affects the amplitude and velocity of the wave allowing SAW sensors to directly sense, e.g., mass loads.

Electro-Mechanical Coupling Coefficient: The electro-mechanical coupling coefficient (κ) defines the conversion efficiency of the piezoelectric material between the electrical and mechanical energies, determined by

$$\kappa^{-2} = \frac{input\ energy}{converted\ energy}. \tag{2}$$

A high coupling coefficient reduces the insertion loss caused by the energy conversion, which results in smaller energy consumption as well as larger effective readout distance of a SAW-based wireless sensor.

SAW Delay Line: The SAW delay line refers to the area between the input IDT and output IDT on the substrate (Fig. 1). It creates a time delay between the input signal and the output signal depending on the SAW velocity and the length of the delay line. Due to this feature, SAW devices are widely used in RF electronics. It is also used in sensing applications, where the measurand causes, e.g., a change in the SAW.

Temperature Coefficient of Delay (TCD): The TCD reflects the temperature dependence of the time delay and is connected with the thermal expansion coefficient (α) and the temperature coefficient of the phase velocity (TCV) by

$$TCD = \alpha - TCV \ . \tag{3}$$

The temperature dependence of the time delay is the basis of SAW temperature sensors, where higher TCD values yield higher sensitivity. However, for other SAW devices, the influence of the TCD on the time delay is undesirable and has to be minimized or eliminated. For this purpose, temperature compensated cuts of the crystalline substrates are employed, where the TCD is minimized over certain temperature ranges [19-20]. Piezoelectric bi-layers are another concept that has been utilized in order to compensate the TCD in sensing applications [21, 22].

2.2. Basic design concepts of passive SAW sensors

Passive SAW sensors typically operate as resonators, delay lines or loaded transponders. In case of resonators, the reflection of the interrogation signal from the SAW device is a function of the SAW device's resonant frequency, which depends on the measurand. In case of delay lines, the request signal is separated from the response signal by a time difference, whereby this time difference depends on the measurand. Similarly, the request signal and response signal are separated by a time difference in case of a loaded transponder. However, the time difference is constant and the measurand affects the signal amplitude. Intrinsic SAW sensors utilize a change of the substrate's properties. For example, intrinsic temperature sensors were realized by detecting the resonant frequency or phase change of the SAW in materials with large TCD [23]. Intrinsic stress sensors utilize the length change of the delay line caused by mechanical strain applied to the substrate. The stress can be evaluated by measuring the SAW phase shift [24]. Extrinsic SAW sensors can be realized by integrating a SAW device and an additional sensing element. A common extrinsic sensor concept utilizes selective thin films on top of the delay line leading to a change in mass by the measurand [13, 25]. This can be, for example, a thin film with high CO_2 solubility and selectivity [26]. As CO_2 dissolves into the film, the additional mass load causes a detectable phase shift in the SAW. Another extrinsic concept utilizes a sensitive IDT. For example, in case of a magnetostrictive IDT, a magnetic field applied to the sensor causes a change of the resonant frequency [8]. A loaded transponder is another extrinsic design, where the output

IDT is connected to a sensor, which changes the IDT's electrical characteristics as a function of the measurand. An example for a load sensor is a pair of conducting rods placed in the earth with a certain distance from each other. As the water level changes, the resistance between the rods changes, which can be detected as a magnitude and phase change of the signal reflected from the load IDT [27]. Another example for a load is a giant magnetoimpedance sensor [16, 17]. A change in the magnetic field yields a change in the sensor's impedance. Consequently, changes the reflectivity of the output IDT.

Some SAW sensors, their classification and method of detection are presented in Table 1.

Sensor Type	Commercialization	Year	Intrinsic/ Extrinsic	Design	Detection Method	Access	Paper
Temperature	Yes	1990	Intrinsic	Resonator	Frequency	None	[23]
		2003	Intrinsic	Delay line	Phase velocity	None	[28]
Pressure	Yes	2001	Extrinsic	Loaded Transponder	Phase	Capacitive pressure sensor	[25]
		2007	Intrinsic	Delay line	Phase	None	[24]
Bio/Chem	No/Yes	2006	Extrinsic	Resonator	Frequency	Thin film	[29]
		2011	Extrinsic	Delay line	Phase	Thin film	[26]
		2001	Extrinsic	Loaded Transponder	Amplitude/ Phase	Conducting rods	[30]
Magnetic	No	1975	Extrinsic	Delay line	Phase	Thin film	[13]
		2011	Extrinsic	Resonator	Frequency	Magnetostrictive IDTs	[8]
		2006/11	Extrinsic	Loaded Transponder	Amplitude	GMI wire/ thin film	[16,17]
Sound	No	2005	Extrinsic	Loaded Transponder	Phase	Capacitive pressure sensor	[31]
Torque	Yes	1996	Intrinsic	Delay line	Phase	None	[32]

Table 1. SAW-based passive sensors.

3. Passive and remote SAW-based magnetic sensors

Magnetic sensors are one of the most versatile sensors employed not only for the task of measuring magnetic fields but for a large number of different applications, thereby detecting the measurand indirectly, e.g., via a change of material parameters in construction monitoring or a change of distance in position monitoring. A passive and remote operation of magnetic sensors can be advantageous in many cases and considerably increase their applicability.

A SAW-based passive magnetic sensor can be realized either by adding an additional material layer, which is sensitive to magnetic fields, or by loading the output IDT with a magnetic sensor. In the first case, the magnetic layer changes the delay line or the resonant frequency of the SAW device. While in the second case, the sensor changes the reflection

signal of the output IDT. Since SAW devices are operated by RF power, the sensor element has to work at the operation frequency of the SAW device. Among the available magnetic sensors, GMI sensors are the most suitable candidates as they have a high magnetic sensitivity as well as a high operating frequency.

3.1. Magnetostrictive SAW devices

Magnetostriction defines the relationship between the strain and the magnetization states of a material. It is an important property of ferromagnetic materials and was first observed by James Joule in 1842 in nickel samples. For a positive/negative magnetostrictive material, an applied magnetic field causes the material to expand/shrink in the field direction. Inversely, when a stress is applied to the magnetostrictive material, its magnetic anisotropy will change accordingly.

A magnetostrictive-piezoelectric resonator consists of amorphous magnetostrictive material layers as the electrodes sandwiching a piezoelectric core (Fig. 2). An ac signal applied to the electrodes causes the quartz layer to oscillate. The resonant frequency of this oscillation depends on the thickness of the piezoelectric material, the crystal orientation, temperature and mechanical stress, etc.

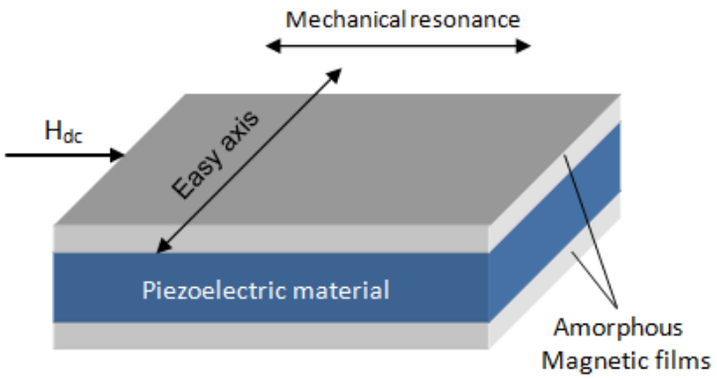

Figure 2. Structure of a composite magnetostrictive/piezoelectric resonator. The magnetic anisotropy is perpendicular to the external magnetic field H_{dc}.

When a magnetic field H_{dc} is applied, the length change induced in the magnetostrictive film exerts stress to the piezoelectric material and, consequently, shifts the resonant frequency of the device. Utilizing this concept, a magnetic sensitivity high enough to detect the terrestrial field has been achieved [33]. In a similar work, a magnetostrictive-piezoelectric tri-layer structure has been embedded in a coil. The dc magnetic field sensitivity was as high as 10^{-8} T [34].

3.1.1. Passive resonator

A SAW-based, passive resonator for magnetic field detection was developed recently by Kadota et al [8]. Nickel, which is a negative magnetostrictive material, was used to fabricate the sensing IDT on a quartz substrate (Fig. 3). Upon the application of a magnetic field,

stress will be induced to the substrate by the IDT change causing a change in the resonant frequency. This sensor showed a frequency change of 200 ppm for a magnetic field of 100 mT applied perpendicularly to the direction of SAW propagation.

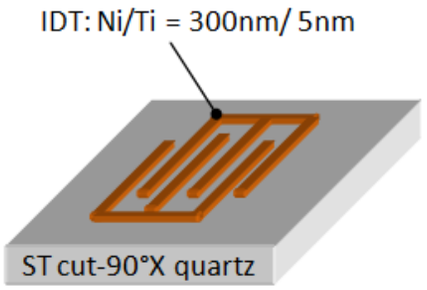

Figure 3. Schematic of a magnetic sensor device using a magnetostrictive IDT on a SAW substrate.

3.1.2. Passive phase shifter

A magnetically tuned SAW phase shifter is a one-port SAW structure with a magnetic sensing functionality achieved through a delay line sensitive to magnetic fields. This idea was first introduced by Ganguly et al in 1975 [13]. In their device, the acoustic velocity is varied by an external magnetic field. This functionality is facilitated by a magnetostrictive thin film deposited on top of the delay line (Fig. 4). The propagation velocity of the SAW in the film region depends on the magnetic field. Hence, there is a correlation between the time shift of the reflected signal and the magnetic field.

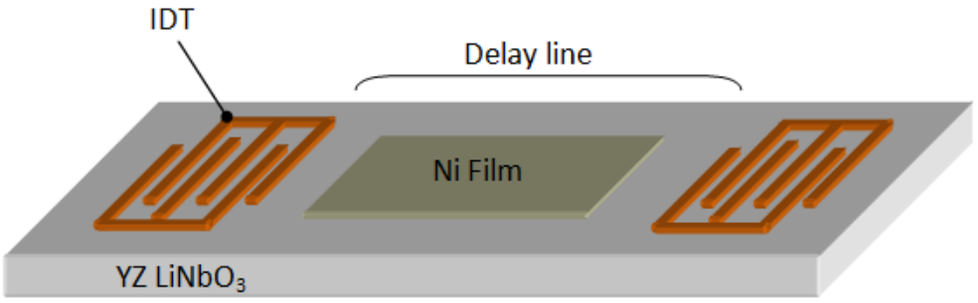

Figure 4. Schematic of a magnetically tuned SAW wave phase shifter.

Later, research efforts focused on different magnetostrictive materials and measurement methods [9, 35, 36], and a magnetic sensitivity of 10^{-4} %/kOe was achieved.

3.2. SAW-GMI sensors

A SAW-based, magnetic and passive sensors comprises a two-port SAW transponder and a magnetic sensor acting as a load at the output IDT. Among the available magnetic field sensors, giant magnetoimpedance (GMI) sensors offer favorable characteristics like high sensitivity to magnetic fields and high operation frequency (compatible with SAW

transponders) making them a very suitable load. SAW-GMI sensors have been fabricated by combining SAW transponders with GMI wire sensors as well as thin film GMI sensors. Both of these methods have shown a higher magnetic sensitivity than direct designs.

3.2.1. Basics of GMI sensors

The GMI effect was first observed in Co-based amorphous wires by Panina and Mohri in 1994 [37] and has since attracted strong interest due to its sensitivity enabling magnetic field measurement with a nT resolution. The GMI effect is the impedance change of an ac-powered ferromagnetic conductor upon the change of a magnetic field. The relative impedance change, also called GMI ratio, is expressed as

$$\text{GMI Ratio (\%)} = 100\% \times \frac{Z(H)-Z(H_0)}{Z(H_0)} \quad \text{or} \quad \text{GMI Ratio (\%)} = 100\% \times \frac{Z(H)-Z(H_{max})}{Z(H_{max})}, \tag{4}$$

where $Z(H_0)$ is the impedance at zero magnetic field and $Z(H_{max})$ is the impedance at saturation field. Both definitions have particular aspects that should be considered. In case of the first expression, $Z(H_0)$ depends on the remanent state of the magnetic material while, in the second case, $Z(H_{max})$ is not always achievable and equipment dependent.

The GMI effect is explained by classical electromagnetism. The change of the complex impedance mainly originates from the skin effect in conjunction with a change of the complex permeability. Analytically, the complex impedance (Z) of a conductor is defined by

$$Z = \frac{U_{ac}}{I_{ac}} = \frac{\int_L \frac{1}{\sigma} \boldsymbol{J_z}(S)dz}{\iint_q \boldsymbol{J_z} dq}, \tag{5}$$

where U_{ac} is the applied ac voltage, I_{ac} is the current, L is the length and σ the conductivity. S and q refer to the surface and the cross section of the conductor, respectively. J_z is the current density in the longitudinal direction obtained by solving Maxwell's equations. In ferromagnetic materials, by neglecting displacement currents ($\dot{\boldsymbol{D}} = \boldsymbol{0}$), Maxwell's equations can be written as follows:

$$\nabla \times \boldsymbol{H} = \boldsymbol{J}, \tag{6}$$

$$\nabla \times \boldsymbol{J} = -\frac{\mu_0}{\rho_f}(\dot{\boldsymbol{H}} + \dot{\boldsymbol{M}}), \tag{7}$$

$$\nabla \cdot (\boldsymbol{H} + \boldsymbol{M}) = 0, \tag{8}$$

J is the current density, H is the applied magnetic field, M is the magnetization of the ferromagnetic material, ρ_f is the free charge density and μ_0 is the permeability of vacuum. From Equ. (6) to (8), the expression

$$\nabla^2 \boldsymbol{H} - \frac{\mu_0}{\rho_f}\dot{\boldsymbol{H}} = \frac{\mu_0}{\rho_f}\dot{\boldsymbol{M}} - \nabla(\nabla \cdot \boldsymbol{M}), \tag{9}$$

can be derived. Equ. (9) can be solved using the Landau-Lifshitz equation, which relates $\boldsymbol{M}$ and $\boldsymbol{H}$

$$\dot{\boldsymbol{M}} = \boldsymbol{\gamma M} \times \boldsymbol{H}_{eff} - \frac{\boldsymbol{\alpha}}{\boldsymbol{M}_s} \boldsymbol{M} \times \dot{\boldsymbol{M}}, \tag{10}$$

where γ is the gyromagnetic ratio, M_s is the saturation magnetization, α is the damping parameter and H_{eff} is the effective magnetic field expressed as [30]

$$\boldsymbol{H}_{eff} = \boldsymbol{H} + \boldsymbol{H}_{\mathbf{a}} + \frac{2A}{\mu_0 M_s} \nabla^2 \boldsymbol{M} \tag{11}$$

where $\boldsymbol{H}$ is the internal magnetic field that includes the applied field and demagnetizing field, $\boldsymbol{H}_a$ is the anisotropy field and A is the exchange stiffness constant..

By combining Equ. (5) to (11), a theoretical impedance model can be evaluated for GMI sensors with different geometries [37-40].

Although the experimentally obtained GMI effect shows a large sensitivity compared to other effects exploited for magnetic sensors, the theoretically estimated values have not been achieved yet. Therefore, a lot of effort has been put into improving the magnetic properties of GMI materials [41-44]. At the same time, GMI sensors of different structures have been developed such as glass-coated wires, thin films, multi layer thin films, meander structures, ribbons, etc. [45-47]

3.2.2. Wire GMI sensors

As the first discovered GMI sensor structures, GMI wire sensors have been extensively studied. Based on the classical electromagnetism, the theoretical model of the GMI wire is (Panina et al, 1994) [37]

$$Z = \frac{R_{dc} kr \zeta_0(kr)}{2\zeta_1(kr)}, \tag{12}$$

where

$$k = \frac{1+j}{\delta_m} \tag{13}$$

and

$$\delta_m = \frac{c}{\sqrt{4\pi^2 f \sigma \mu_\emptyset}}. \tag{14}$$

R_{dc} is the dc resistance of the wire, ζ_0, ζ_1 are the Bessel functions, r is the radius of the wire, j is the imaginary unit, δ_m is the penetration depth, c is the speed of light, f is the frequency of the ac current, $\mu_\emptyset$ is the circumferential magnetic anisotropy. The origin of the GMI effect lies in the dependence of $\mu_\emptyset$ on an axial magnetic field resulting in a change of δ_m. In order to obtain a high GMI ratio, the value of δ_m has to be close to the thickness of the conductor. Hence, the thinner a ferromagnetic conductor and the lower its permeability, the higher the operation frequency required. A well-defined circumferential magnetic anisotropy in combination with a soft magnetic behavior is desirable, since it will provide a large permeability change for small magnetic fields.

Different amorphous and ferromagnetic materials were used to fabricate GMI wires [48], and various fabrication methods were developed such as melt spinning, in-rotating water spinning, glass-coated melt spinning etc. [45, 49, 50]. Glass-coated micro-wires (Fig. 5) present outstanding properties in terms of the magnetic anisotropy distribution, which is reinforced by the strong mechanical stress induced by the coating. $(Co_xFe_{1-x})_{72.5}Si_{12.5}B_{15}$ is one of the most typical materials. By adjusting x from 0 to 1, the magnetostriction of the material changes from positive at high Fe content to negative at high Co content. Negative magnetostrictive compositions in combination with the compressive, radial stress induced by quenching and the glass coating provide the best results, since it supports a strong circumferential anisotropy.

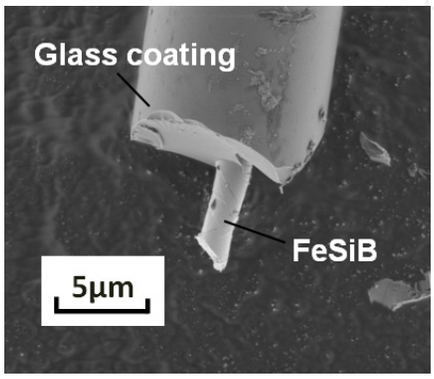

Figure 5. SEM image of a glass-coated amorphous micro-wire (Courtesy of M. Vazquez, Inst. Materials Science of Madrid, CSIC).

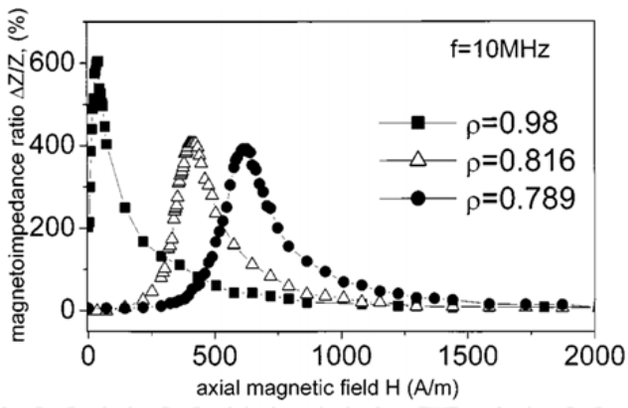

Figure 6. GMI ratio of $Co_{67}Fe_{3.85}Ni_{1.45}B_{11.5}Si_{14.5}Mo_{1.7}$ glass-coated wires with different geometric ratio ρ (the metallic nucleus diameter to the total microwire diameter) at 10 MHz.

Wire-type GMI sensors provide the best performance in terms of the GMI ratio with values as high as 615% (Fig. 6) achieved with optimized glass coated microwires (Zhukova et al, 2002) [43]. The value of the magnetic field at which the maximum GMI ratio is obtained increases as the diameter of the magnetic nucleus decreases compared to the diameter of the glass coating. This is attributed to the different anisotropies induced by the stress from the coating. Due to the high sensitivity provided by GMI wires they have been commercialized despite the facts that fabrication is not silicon based, does not use standard microfabrication methods and, as a consequence, integration with electronics is complex.

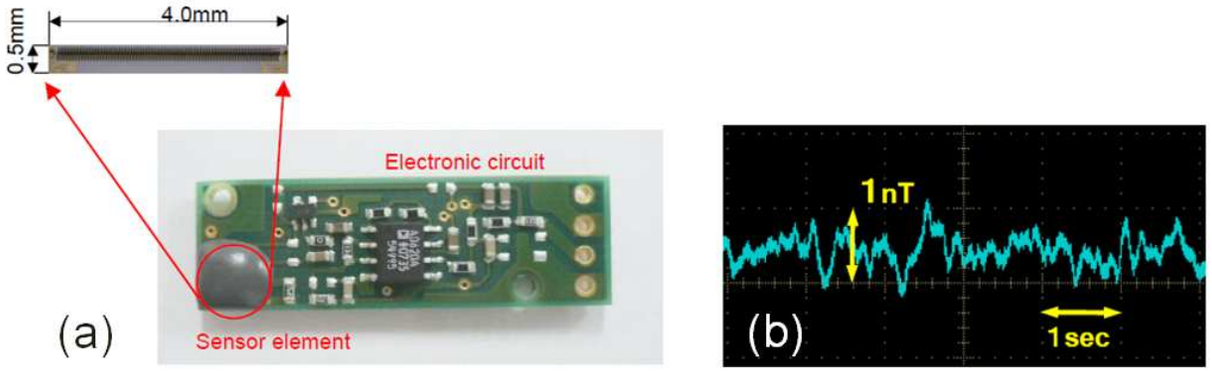

Figure 7. (a) Layout of the commercialized GMI sensor from Aichi Steel Co. (b) Noise output of the GMI sensor.

Fig. 7 shows a GMI sensor developed by Aichi Steel Co., which has a very high sensitivity of 1 V/μT and a noise level of 1 nT [51].

3.2.3. Ribbon GMI sensors

Magnetic ribbons discussed in this section are planar structures of rectangular shape with a thickness of a few tens of micrometers and a length and width from several millimeters to centimeters. Similar to the micro-wires, magnetostriction is utilized in order to create certain anisotropies during the ribbon's fabrication. Magnetic ribbons that exhibit a strong GMI effect have a high permeability as well as a transversal magnetic anisotropy.

For a planar film of infinite width, the impedance is given by

$$Z = R_{dc} \cdot \frac{jka}{2} coth(\frac{jka}{2}) , \tag{15}$$

where R_{dc} is the dc resistance, a is the thickness of the ribbon, k and δ_m can be obtained from Equ. (14) with the only difference that $\mu_{ø}$ represents the transversal permeability instead of the circumferential one [52].

Again, Fe- and Co-based amorphous alloys are preferably used as the magnetic material. The standard fabrication method for the ribbons is melt spinning, where a rotating copper wheel is used to rapidly solidify the liquid alloy. This method produces magnetic ribbons with a thickness of about 25 μm and a width of several mm. With this thickness, ribbon GMI sensors operate at comparably low frequencies of hundred kHz up to a few MHz. A GMI ratio of, e.g., 640% has been obtained with a GMI ribbon made of $Fe_{71}Al_2Si_{14}B_{8.5}Cu_1Nb_{3.5}$ at 5 MHz [53].

3.2.4. Thin film GMI sensors

In theory, a single layer magnetic thin film is similar to a magnetic ribbon, and the same analytical expressions are applied for modeling the GMI effect. Practically, the main difference is the fabrication method. Thin film fabrication is a standard micro-fabrication

technology producing a film thickness of some nanometers up to a few micrometers. Thin film GMI sensors are of great interest due to the advantages arising from the fabrication in terms of the flexibility in design and integration. They can easily be fabricated on the same substrate as the electronic circuit and other devices. In the context of passive and remote sensors, this is particularly relevant, since the GMI element can be easily integrated with an SAW device. For this reason, GMI thin film sensors will be discussed in more detail and our recent results will be presented.

Compared to wires and ribbons, the results obtained with thin film sensors have not been as good, and the highest GMI ratios reported are around 250% [42]. This may be due to the differences in the magnetic softness as well as the magnetic anisotropy, which is very well established in circumferential and transversal direction in wires and ribbons, respectively, and is difficult to control in thin films. In thin films transverse anisotropy is mainly realized through magnetic field deposition or field annealing, Fig. 8 (a) and (b) show the magnetization curve and domain structure of a $Ni_{80}Fe_{20}$ thin film (100nm thick) fabricated under a magnetic field of 200 Oe during deposition. A magnetic easy axis and domain structures in transverse direction are observed. Due to the small thickness, thin film GMI sensors normally operate at a higher frequency from hundred MHz to several GHz where the penetration depth is in the range of the film thickness.

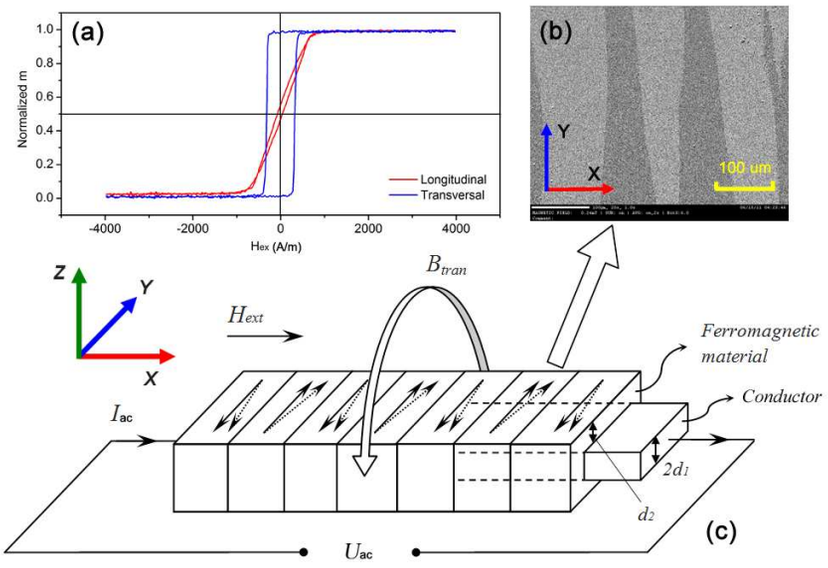

Figure 8. (a) Magnetization curves obtained by vibrating sample magnetometry of a magnetic thin film (100nm of $Ni_{80}Fe_{20}$) in transversal and longitudinal directions. (b) Domain pattern of the magnetic layer. (c) Schematic of a typical multi layer GMI structure. The arrows in the ferromagnetic material indicate the magnetization of individual domains (simplified). Upon application of an external magnetic field H_{ext}, the magnetization rotates into the direction of H_{ext} (dotted arrows).

In general, a GMI sensor with high sensitivity consists of a stack of several material layers. In case of a tri-layer element, one conducting layer is sandwiched between two magnetic layers as shown in Fig. 8 (c). The conducting layer ensures a high conductivity and, in combination with the highly permeable magnetic layers, a large skin effect is obtained [51,

54]. An alternating current I_{ac} mainly flowing through the conductor generates a transversal flux B_{tran}, which magnetizes the magnetic layers. Upon the application of an external field H_{ext} in longitudinal direction, the magnetization caused by I_{ac} will be changed. This is equivalent to a change of the transversal permeability of the magnetic layers and is reflected by an impedance change.

The analytical model of the impedance for a magnetic/conducting/magnetic tri-layer structure is given by

$$Z = R_{dc}(1 - 2j\mu\frac{d_1 d_2}{\delta_c^2}), \tag{16}$$

where R_{dc} is the dc resistance of the inner conductor, $2d_1$ is the thickness of the conductor, d_2 is the thickness of the magnetic layers as shown in Fig. 8 (c) and δ_c is the penetration depth of the conducting layer [39].

Analytical solutions for the impedance of thin film GMI sensors can only be found for rather simple structures. In order to calculate the impedance of more complicated geometries, for example, a sandwich structure with isolation layers between the conductor and the magnetic layers [41], a meander structure multilayer [46] or to take into account edge effects, the finite element method (FEM) provides a viable solution [55].

Fig. 9 shows the comparison of the GMI ratios simulated for a single magnetic layer, a tri-layer structure made of a magnetic/conducting/magnetic stack and a five-layer structure with isolation layers between the conducting and magnetic layers using the FEM. The simulated GMI sensors have a width of w = 50 μm and length of l = 200μm. The magnetic layers have a thickness of t_{mag} = 1 μm and the conducting layer has a thickness of t_{met} = 4 μm. The material of the isolation layer is SiO_2 with a thickness of 1μm. The conductivity of the ferromagnetic and conducting layers are 7.69×10^5 S/m $((CoFe)_{80}B_{20})$ and 4.56×10^7 S/m (Gold), respectively. All parameters including M_s = 5.6×10^5 A/m, γ = 2.2×10^5 m/(A·s), α = 0.3, H_a= 1890 A/m and are taken from literature [56].

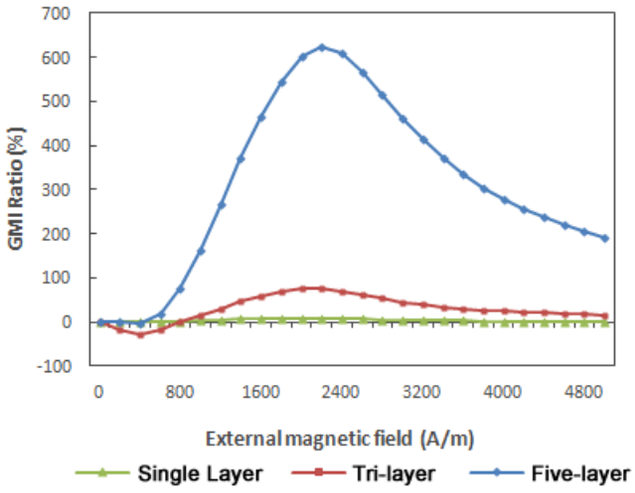

Figure 9. Simulated GMI ratios of single layer, sandwiched multilayer and isolated sandwiched multilayer structures.

The results clearly show the performance increase achieved with the multilayer structures. Specifically, the isolated sandwich structure has a superior performance, which is due to preventing the current from flowing in the magnetic layer.

For the fabrication of thin film GMI sensors, Co-based and Fe-based amorphous magnetic alloys were used in earlier studies. Recently, permalloy, which is a NiFe compound, became popular as it provides very high permeability, zero magnetostriction and simple fabrication. Meander shaped multilayers and different stacks of magnetic and conductive layers using permalloy were developed. Some results are summarized in Table 2.

Year	Material	Frequency	GMI Ratio (%)	Sensitivity (%/Oe)	Reference
1999	FeNiCrSiB/Cu/FeNiCrSiB	13MHz	77	2.8	[57]
2000	FeSiBCuNb/Cu/FeSiBCuNb	13MHz	80	2.8	[58]
2004	$Ni_{81}Fe_{19}$/Au/$Ni_{81}Fe_{19}$	300MHz	150	30	[59]
2004	($Ni_{81}Fe_{19}$/Ag)n	1.8GHz	250	9.3	[42]
2005	FeCuNbSiB/SiO_2/Cu/SiO_2/FeCuNbSiB	5.45MHz	33	1.5	[60]
2011	NiFe/Ag/NiFe	1.8GHz	55	1.2	[61]
2011	NiFe/Cu/NiFe	20MHz	166	8.3	[62]

Table 2. Recent results on thin film GMI sensors.

GMI thin film sensors not only offer the advantages of standard microfabrication and straight-forward integration with SAW devices, but, as can be seen from Table 2, the operation frequency of GMI thin film sensors is also compatible with the one of SAW devices (usually from hundred MHz to several GHz and can be adjusted within a wide range.

3.2.5. Integrated SAW-GMI sensor

In the first studies, SAW transponders and GMI wire sensors were combined to form remote devices [14-16]. GMI wires were selected for their high sensitivity, and they were bonded to the output IDT of the SAW device, which operated as a reflector, in order to act as load impedance. The strong dependence of the impedance on magnetic fields causes a considerable amplitude dependence of the reflected signal on magnetic fields. Even though these studies provided good results for passive and remote magnetic field sensors, the fabrication method for the GMI wires, which is not compatible with standard microfabrication, is a considerable problem with respect to reproducibility and costs, hence, hindering commercial success of such devices. In order to conquer this problem, a fully integrated SAW-GMI design utilizing standard microfabrication processes is required. The most viable option is a thin film GMI sensors for the following reasons:

1. Thin film GMI sensors can be produced by the same metallization processes as the SAW transponders and on the same substrate.

2. Standard photolithography technique guarantees an accurate and reproducible alignment of the two devices.
3. Thin film GMI sensors provide a wide range of working frequencies up to GHz, which matches the high frequency requirement of the SAW transponders.
4. Thin film GMI sensor can have a minimized and flexible design as well as large magnetic field sensitivity.

In this section, a detailed description of our recent work on the design, fabrication and testing of an integrated SAW-GMI sensor is presented.

Design

Fig. 10 shows a schematic of a GMI thin film sensor integrated with a SAW transponder. A wireless signal applied to the source IDT (IDT1) is converted to an SAW and propagates towards the other end of the substrate, where it is reflected from the reference IDT (IDT2) and the load IDT (IDT3). The reflected waves containing the reference and load information are received by IDT1 at different time instants and reconverted to a wireless electrical signal sent out via the antenna.

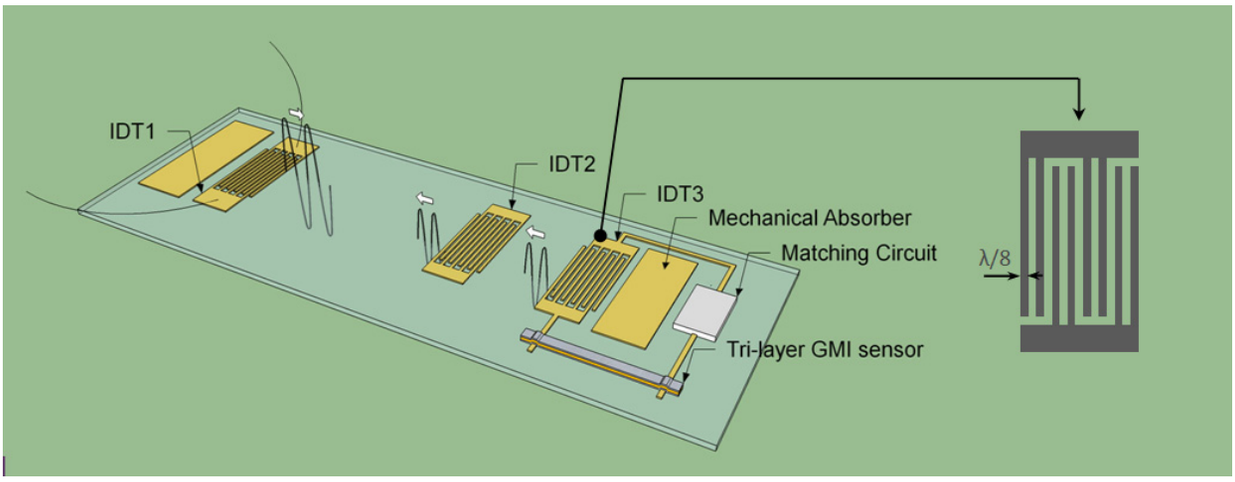

Figure 10. Schematic of an integrated passive and remote magnetic field sensor consisting of a SAW transponder and thin film GMI sensor.

In order to obtain high magnetic field sensitivity, the GMI sensor is matched to the output port (IDT3) at the working frequency of the SAW device. As the impedance of the GMI sensor changes with an applied magnetic field, the matching deteriorates, which causes the amplitude of the signal reflected from IDT3 to change. Since the piezoelectric material is sensitive to environmental changes, e.g. temperature, a reference IDT is used to provide a signal that enables the suppression of such noise by means of signal processing. Two metallic pads next to the input and output IDTs act as mechanical absorbers and suppress reflections from other structures on the substrate or the edge of the substrate.

Matching the sensor load to the optimal working point of IDT3 is a crucial aspect in the device design. Therefore, the influence of the load on the signal reflected from IDT3 is simulated. The interaction of a SAW with an IDT can be described by the P-matrix model

introduced by Tobolka [63]. As shown in Fig. 11, P_{11} is the acoustic wave reflection at the output IDT [24]. Specifically, the dependence of P_{11} on the load impedance $Z = Z(H_{ext}) + Z_m$, where $Z(H_{ext})$ is the impedance of the GMI element and Z_m is the matching impedance, is expressed as

$$P_{11}(Z) = P_{11,sc} + \frac{2 \cdot P_{13}^2}{P_{33} + \frac{1}{Z}}, \tag{17}$$

where $P_{11,sc}$ is the short circuit reflection coefficient, P_{13} is the electro-acoustic transfer coefficient and P_{33} is the input admittance of the transducer. In order to have a large change of P_{11}, which is equivalent to the sensitivity of the SAW device loaded by an impedance sensor, the influence of Z in equation (17) needs to be large. Therefore, a SAW transducer with a small $P_{11,sc}$ and large P_{13} will provide a large sensitivity. $P_{11,sc}$ can be minimized by using a double electrode IDT design as shown in Fig. 10, which provides cancelation of the internal mechanical reflections of the IDT.

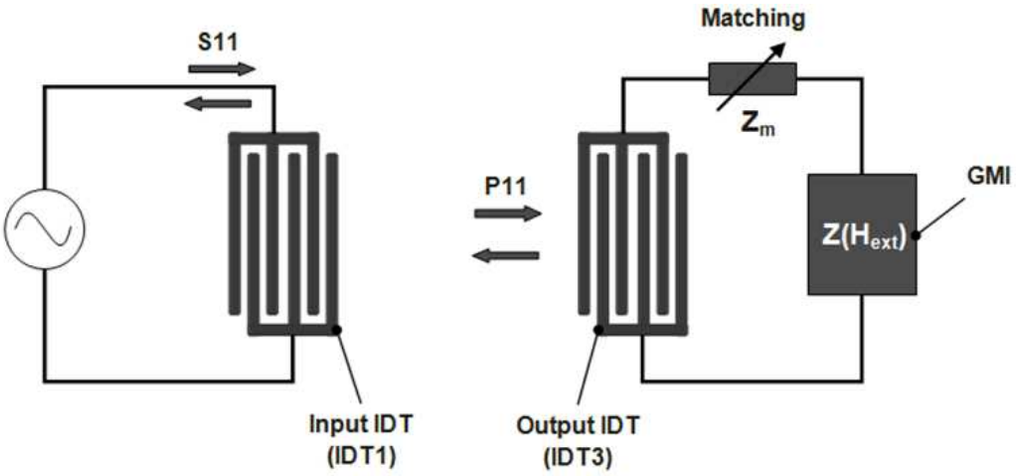

Figure 11. Electric and acoustic ports of the SAW sensor

The electro-acoustic transfer coefficient P_{13} and input admittance P_{33} can be obtained by,

$$P_{13} = \frac{1}{2\sqrt{2Z_a}} r_m (1 - e^{-j\varphi_m}) \tag{18}$$

$$P_{33} = j\omega C_{IDT} + \frac{r_m^2}{Z_a}(1 - e^{-j\varphi_m}) \tag{19}$$

Where r_m is the ratio of the electrical to acoustical transformer, C_{IDT} is the capacitance of the IDT, Za is the acoustic impedance and φ_m is the transit angle [63].

Since the GMI sensor is an inductive element, matching is accomplished by a series capacitance resulting a load impedance

$$Z = 1/j\omega C_m + R + j\omega L(H_{ext}), \tag{20}$$

where C_m is the matching capacitance, R is the average resistance (over the considered magnetic field range) of the GMI sensor and $L(H_{ext})$ the inductance of the GMI sensor.

Fig. 12 (a) shows the simulation result of the IDT's reflectivity as a function of the load. The slope of this plot corresponds to the magnetic field sensitivity. Therefore, the optimum matching capacitance can be determined. Fig. 12 (b) presents the rate of change of P_{11} for 1nH inductance changes (corresponding to a field change of approximately 50A/m). The result shows that with the optimum matching capacitance a maximum reflectivity change rate of 0.3dB/nH can be achieved. As the fabricated GMI sensor has an inductance change from 5nH to 15nH, a reflectivity change of 3dB can be expected.

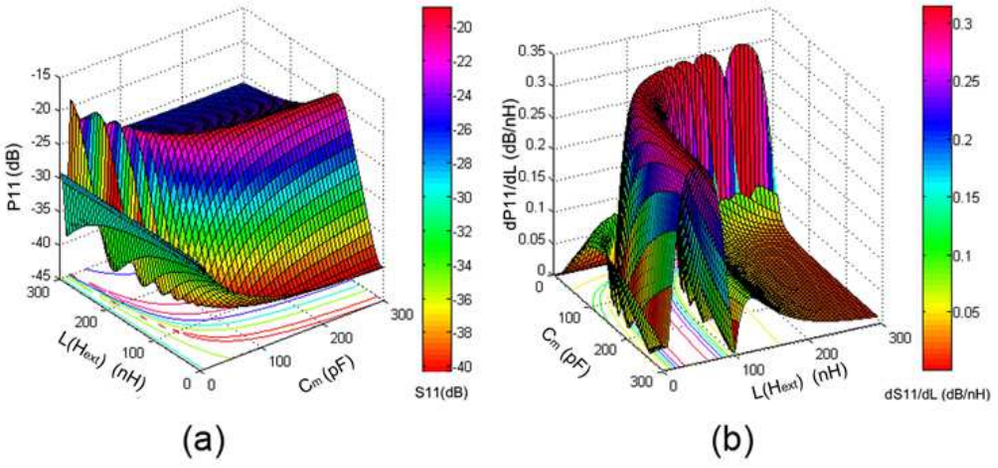

Figure 12. (a) Magnitude P_{11} as a function of the matching capacitance and sensor inductance. (b) Rate of change (absolute value) of P_{11} for 1nH load inductance change.

The piezoelectric substrate chosen for this application is $LiNbO_3$ as it provides a strong electromechanical coupling corresponding to a high value of P_{13}. The detailed design parameters of the SAW transponder are shown in Tab. 3. The working frequency of the device is 80MHz, resulting in a periodicity p of 50µm (Equ. (1). The value of p determines the electrode width and gap. The distances between the IDTs yield a 1.25µs delay between IDT1 and IDT2 and a 0.625µs delay between IDT2 and IDT3.

Design parameter		Design parameter	
Substrate material	$LiNbO_3$ (128 deg. Y-X cut)	Electrode material	Gold
Center frequency	80MHz	Aperture	30λ
Periodicity	50µm	Electrode/gap width	6.25µm
Electrodes per segment	4	IDT segment number	30

Table 3. Design parameters for the SAW device.

The GMI sensor consists of a tri-layer structure with two ferromagnetic layers of 100nm in thickness made of $Ni_{80}Fe_{20}$ and a conducting copper layer with a thickness of 200nm. The

sensor has a rectangular geometry of 100 μm× 4000 μm. The conducting layer is connected to the IDT3 [18].

Fabrication

The fabrication of the combined device is accomplished in several steps as shown in Fig. 13. On a $LiNbO_3$ wafer, a 40 nm Ti adhesion layer and 200 nm gold layer are sputter deposited and patterned by ion milling into individual SAW devices. The leads and SMD footprints are designed together with the SAW device to facilitate an on-chip impedance matching circuit, which was accomplished by a 150pF capacitor connected in series with the GMI element. The GMI element comprises a tri-layer structure ($Ni_{80}Fe_{20}$(100nm) / Cu(200nm) / $Ni_{80}Fe_{20}$(100nm)) deposited at room temperature with a uniaxial magnetic field of 200 Oe applied in the transversal direction.

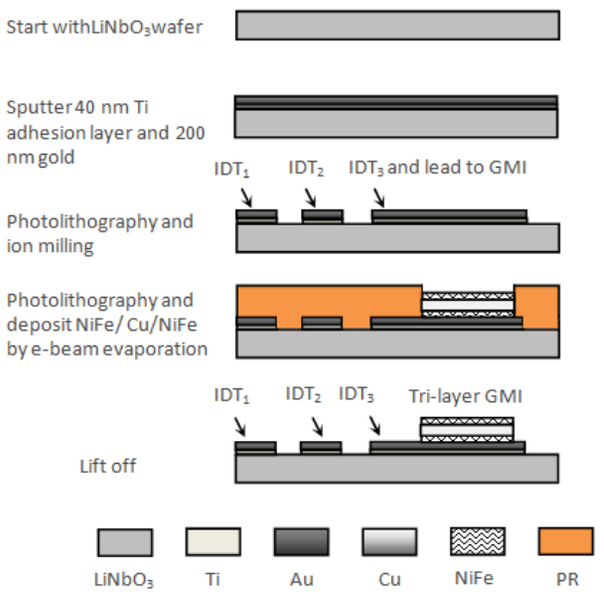

Figure 13. Fabrication flow chart of the integrated SAW-GMI device.

Results

A network analyzer (Agilent E8363C) is used to apply an RF signal to IDT1 and measure the electric reflection coefficient (S_{11}) of the input IDT, which is related to the admittance matrix of the whole device and P_{11}. The time domain signal of S_{11} is converted from the frequency domain using fast Fourier transform. As shown in Fig. 14 (a), two reflection peaks at 2.45μs and 3.55μs are observed indicating the reflections from the reference IDT and the load IDT accordingly. The magnetic response of the integrated device is determined by applying a variable magnetic field in longitudinal direction to the device. A 2.4dB amplitude change of the reflection signal can be observed. A comparison of the simulated and experimental results together with the measured GMI ratio curve is shown in Fig. 14 (b).

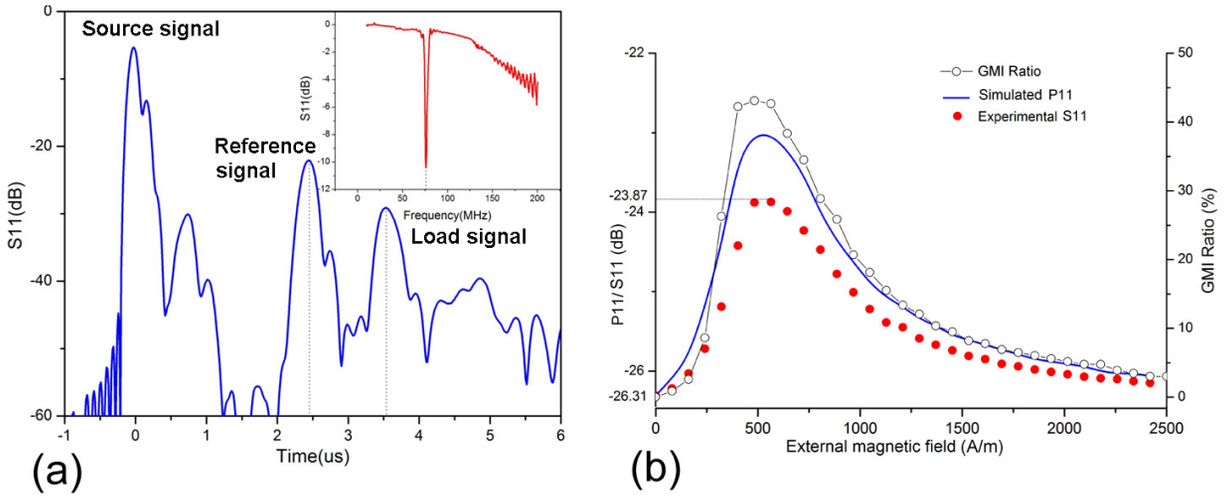

Figure 14. (a) Time domain measurement of the SAW-GMI device. Inset: Frequency domain measurement. (b) Comparison of the simulated and experimental device response together with the measured GMI ratio curve.

4. Potential applications

Magnetic field sensors are one of the most widely used sensors and employed for many different applications. Current commercial magnetic sensors are wire connected to a circuit providing power and readout. These wire connections prevent the sensors from being used for certain applications. In addition, as the complexity and the number of devices, increases in modern systems such as automobiles, wire connections are becoming an increasing problem due to limited space. For those and other reasons, wireless solutions are being much sought after.

As pointed out in the previous sections, SAW-based sensors have been developed for different applications, and this technology also provides a platform for realizing wireless and passive magnetic sensors. They can provide solutions for various applications, for example, where the sensors have to withstand harsh environmental conditions or are required to have a long lifetime without maintenance.

Out of the countless applications for SAW-based passive and remote magnetic field sensors, a few will be highlighted in the following.

Nanotechnology and miniaturized systems are becoming increasingly popular in the biomedical field. Technologies based on magnetic effects are of particular interest since they can be controlled remotely via magnetic fields. For example, NVE Corporation recently developed a battery operated magnetic sensor to be used as a magnetic switch for implantable devices. When a magnetic field is applied, the sensor turns on triggering a specified action. It turns off when the field is removed. The sensor works at a stable operating point of 15 Oe [64]. Magnetic beads have been extensively used in many biomedical applications. These magnetic beads are made of ferromagnetic material ranging in size between 5 nm to 500 um. A new application of such particles promises benefits in

cancer therapy by employing the particles either as drug carriers or heat sources (hyperthermia) [65]. In order to have better control of the treatment, magnetic sensors are considered to measure and detect the concentration of these magnetic particles.

The automotive industry extensively uses magnetic sensors for different purposes, for example, to measure current in electric vehicles [66] or the rotation speed of gears [67]. Another application employs magnetic sensors to detect passing vehicles using lane markers [68]. Such a system could also be used to detect vehicle speed by measuring the time between two markers of a fixed distance. In yet another application, developed by Stendl et al [69], the wear of a vehicle's tire is detected by measuring the field of magnetic beads embedded in the rubber of tire treads. As the tread size decreases, the magnetic field also decreases. A wireless magnetic sensor is placed just below the threads.

Construction monitoring is an upcoming application for wireless sensor. Long-term monitoring of metallic reinforcements in, e.g., bridges or buildings requires passive and remote sensors, which are capable of detecting changes of the metal. Similarly, the detection of internal defects or corrosion of pipelines is of great interest. Gloria et al [70] developed an Internal Corrosion Sensor (ICS) consisting of a magnet and a Hall sensor. A disturbance in the magnetic field caused by changes of the metal changes the sensor readout. This information is used for both to detect and size the defects.

5. Conclusion

In this chapter we discussed different types of SAW-based, magnetic sensors including resonators, phase shifters and loaded transponders. Sensitivity to magnetic fields can be achieved by either changing the properties of the IDT or delay line utilizing magnetostrictive materials or loading the output IDT with a magnetic field sensor. GMI sensors feature a very high sensitivity and wide range of operating frequencies and, therefore, constitute an especially suitable load. The principle of GMI sensors is described in detail and different GMI structures are discussed. While the highest sensitivity has been obtained with GMI microwires, thin film GMI sensor are advantageous because they can be produced using standard microfabrication methods, and they can be easily integrated with a SAW transponder on the same substrate. These features are crucial with respect to production complexity and costs.

A SAW transponder combined with a GMI element connected to the output IDT is a passive and remote magnetic field sensor, which responds to an interrogation signal with a delayed response signal. The design of such a device needs to take into account different aspects like operation frequency, dimensions of IDTs and delay line or matching the load with the output IDT. In order to obtain a high sensitivity, an impedance change of the GMI element caused by a magnetic field, has to yield a large change in the SAW reflected from the output IDT. A model is presented to simulate the electro-acoustic interaction of the output IDT with the GMI sensor's impedance and the impedance matching capacitance. The simulation results provide information regarding the matching parameters and are invaluable for

obtaining an optimized performance. A detailed description of the fabrication of an integrated SAW-GMI sensor is provided using standard microfabrication technologies. The GMI ratio of the fabricated sensor is 45 % The SAW-GMI sensor provides a sensitivity of 3 dB/mT, and its output corresponds well with the simulation results.

Magnetic field sensors have countless applications and are widely used in many different fields. The trend towards wireless operation, which is generally observed nowadays, drives the development of passive and remote magnetic field sensors. Several concepts of such sensors employing SAW devices have been presented in this chapter. The most promising one is a SAW-GMI sensor, which has been discussed in detail and which features wireless and battery less operation as well as durability and the ability to withstand harsh environments. This kind of sensor is considerable not only for providing existing applications with a wireless mode; it also largely expands the potential applications of magnetic field sensors.

Author details

Bodong Li and Jürgen Kosel
Electrical Engineering Department, King Abdullah University of Science and Technology, Thuwal, Saudi Arabia

Hommood Al Rowais
Electrical Engineering Department, Georgia Institute of Technology, Atlanta, Georgia, USA

6. References

[1] Stockman H (1948) Communication by means of reflected power, Proceedings of IRE. 36: 1196-1204

[2] Plath F, Schmeckebier O, Rusko M, Vandahl T, Luck H, Moller F, Malocha D C (1994) Remote sensor system using passive SAW sensors. ULTRASON. 1: 585-588

[3] Reindl L, Scholl G, Ostertag T, Scherr H, Wolff U, Schmidt F (1998) Theory and application of passive SAW radio transponders as sensors. IEEE Trans. Ultrason., Ferroelectr., Freq. Control. 45: 1281-1292

[4] Reeder T M and Cullen D E (1976) Surface-acoustic-wave pressure and temperature sensors. Proceedings of the IEEE. 64: 754-756

[5] Lee K, Wang W, Kim G and Yang S (2006) Surface Acoustic Wave Based Pressure Sensor with Ground Shielding over Cavity on 41° YX $LiNbO_3$. Jpn. J. Appl. Phys. 45: 5974–5980

[6] Pohl A (1997) Wirelessly interrogable surface acoustic wave sensors for vehicular applications. IEEE T Instrum Meas. 46: 1031-1038

[7] Calabrese G S, Wohltjen H, Roy M K (1987) Surface acoustic wave devices as chemical sensors in liquids: Evidence disputing the importance of Rayleigh wave propagation, Anal. Chem. 59: 833–837
[8] Kadota M, Ito S, Ito Y, Hada T, And Okaguchi K (2011) Magnetic Sensor Based on Surface Acoustic Wave Resonators. Jpn. J. Appl. Phys. 50: 07HD07
[9] Hanna S M (1987) Magnetic Field Sensors Based on SAW Propagation in Magnetic Films. IEEE Trans. Ultrason., Ferroelectr., Freq. Control. UFFC-34: 191-194
[10] http://www.asrdcorp.com
[11] http://www.senseor.com
[12] http://www.transense.co.uk
[13] Ganguly A K, Davis K L, Webb D C, Vittoria C, Forester D W (1975) Magnetically tuned surface-acoustic-wave phase shifter. *Electronics Letters*. 11: 610-611
[14] Hauser H, Steindl R, Hausleitner Ch, Pohl A, Nicolics J (2000) Wirelessly Interrogable Magnetic Field Sensor Utilizing Giant Magneto-Impedance Effect and Surface Acoustic Wave Devices. IEEE T INSTRUM MEAS. 49: 648-652
[15] Steindl R, Hausleitner Ch, Pohl A, Hauser H, Nicolics J (2000) Passive wirelessly requestable sensors for magnetic field measurements. Sens Actuators A. 85: 169-174
[16] Hauser H, Steurer J, Nicolics J, Musiejovsky L, Giouroudi I (2006) Wireless Magnetic Field Sensor. Journal of Electrical Engineering 57: 9-14
[17] Al Rowais H, Li B, Liang C, Green S, Gianchandani Y, Kosel J (2011) Development of a Passive and Remote Magnetic Microsensor with Thin-Film Giant Magnetoimpedance Element and Surface Acoustic Wave Transponder. J. Appl. Phys. 109: 07E524
[18] Li B, M H. Salem N P, Giouroudi I, Kosel J (2011) Integration of Thin Film Giant Magneto Impedance Sensor and Surface Acoustic Wave Transponder. J. Appl. Phys. 111: 07E514
[19] Sinha B K, Tiersten H F (1979) Zero temperature coefficient of delay for surface waves in quartz. Appl. Phys. Lett. 34: 817
[20] Ebata Y, Suzuki H, Matsumura S and Toshiba K F (1982) SAW Propagation Characteristics on $Li_2B_4O_7$. Jpn. J. Appl. Phys. 22: 160-162
[21] Tsubouchi K.Sugai K, Mikoshiba N (1982) Zero Temperature Coefficient Surface-Acoustic-Wave Devices Using Epitaxial AlN Films. Ultrasonics Symposium, 340 – 345
[22] Dewan N, Tomar M, Gupta V, and Sreenivas K (2005) Temperature stable LiNbO3 surface acoustic wave device with diode sputtered amorphous TeO2 over-layer. Appl. Phys. Lett. 86: 223508
[23] Viens M, Cheeke J D N (1990) Highly sensitive temperaturesensor using SAW resonator oscillator. Sensors and Actuators A: Physical 24: 209-211

[24] Wang W, Lee K, Woo I, Park I, Yang S (2007) Optimal design on SAW sensor for wireless pressure measurement based on reflective delay line. Sensors and Actuators A: Physical. 139: 2-6

[25] Schimetta G, Dollinger F, Scholl G, Weigel R (2001) Optimized design and fabrication of a wireless pressure and temperature sensor unit based on SAW transponder technology. Microwave Symposium Digest, 2001 IEEE MTT-S International. 1: 355-358

[26] Lim C, Wang W, Yang S, Lee K (2011) Development of SAW-based multi-gas sensor for simultaneous detection of CO2 and NO2, Sensors and Actuators B: Chemical. 154: 9-16

[27] Reindl L, Ruppel C C W, Kirmayr A, Stockhausen N, Hilhorst M A, and Balendonck J (2001) Radio-Requestable Passive SAW Water-Content Sensor, IEEE Transactions on Microwave Theory And Techniques. 49: 803

[28] Wang S Q, Harada J and Uda S (2003) A Wireless Surface Acoustic Wave Temperature Sensor Using Langasite as Substrate Material for High-Temperature Applications. Jpn. J. Appl. Phys. 42: 6124

[29] Wu C (2006) Fabrication of Surface Acoustic Wave Sensors for Early Cancer Detection, Electrical Engineering, University of California, Los Angeles

[30] Knobel M, Vazquez M, and Kraus L, Buschow ed. K.H.J. (2003) Giant Magnetoimpedance, Handbook of magnetic materials. 15: 497-563

[31] Sezen A S, Sivaramakrishnan S, Hur S, Rajamani R, Robbins W, and Nelson B J (2005) Passive Wireless MEMS Microphones for Biomedical Applications, J. Biomech. Eng. 127: 1030

[32] Wolff U, Schmidt F, Scholl G, Magori V (1996) Radio accessible SAW sensors for non-contact measurement of torque and temperature. Ultrasonics Symposium Proceedings. 1: 359-362

[33] Yoshizawa N, Yamamoto I, and Shimada Y (2005) Magnetic Field Sensing by an Electrostrictive/Magnetostrictive Composite Resonator. IEEE TRANSACTIONS ON MAGNETICS 41: 11

[34] Dong S, Zhai J, Li J, and Viehland D (2006) Small Dc Magnetic Field Response Of Magnetoelectric Laminate Composites, Applied Physics Letters 88: 082907

[35] Koeninger V, Matsumura Y, Uchida H H, Uchida H (1994) Surface acoustic waves on thin films of giant magnetostrictive alloys. J ALLOY COMPD 211/212: 581-584

[36] Uchida H, Wada M, Koike K, Uchida H H, Koeninger V, Matsumura Y, Kaneko H, Kurino T (1994) Giant magnetostrictive materials: thin film formation and application to magnetic surface acoustic wave devices. J ALLOY COMPD 211/212: 576-580

[37] Panina L V and Mohri K (1994) Magneto-impedance effect in amorphous wires. Appl.Phys.Lett. 65: 1189-1191

[38] Machado F L A, Rezende S M (1996) A theoretical model for the giant magnetoimpedance in ribbons of amorphous soft-ferromagnetic alloys. Journal of Applied Physics. 79: 6558 - 6560

[39] Hika K, Panina L V, Mohri K (1996) Magneto-Impedance in Sandwich Film for Magnetic Sensor Heads. IEEE Trans Magn. 32: 4594-4596.

[40] Panina L V, Makhnovskiy D P, Mapps D J, and Zarechnyuk D S (2001) Two-dimensional analysis of magnetoimpedance in magnetic/metallic multilayers. J. Appl. Phys. 89: 7221

[41] Morikawa T, Nishibe Y, Yamadera H, Nonomura Y, Takeuchi M, Taga Y (1997). Giantmagneto-Impedance Effect in Layered Thin Films. IEEE Trans Magn. 33: 4367-4372

[42] de Andrade A M H, da Silva R B, Correa M A, Viegas A D C, Severino A M, Sommer R L (2004) Magnetoimpedance of NiFe/Ag multilayers in the 100 kHz–1.8 GHz range. Journal of Magnetism and Magnetic Materials 272–276: 1846–1847

[43] Zhukova V, Chizhik A, Zhukov A, Torcunov A, Larin V and Gonzalez J (2002) Optimization of giant magnetoimpedance in Co-rich amorphous microwires. IEEE Trans. Magn. 38: 3090-3092

[44] Le A T, Phan M H, Kim C O, Vázquez M, Lee H, Hoa N Q and Yu S C (2007) Influences of annealing and wire geometry on the giant magnetoimpedance effect in a glass-coated microwire LC-resonator, J. Phys. D: Appl. Phys. 40: 4582–4585

[45] Vázquez M, Adenot-Engelvin A L (2009) Glass-coated amorphous ferromagnetic microwires at microwave frequencies. Journal of Magnetism and Magnetic Materials. 321: 2066–2073

[46] Zhou Z, Zhou Y, Chen L (2008) Perpendicular GMI Effect in Meander NiFe and NiFe/Cu/NiFe Film. IEEE Transactions on Magnetics. 44: 2252 - 2254

[47] Pompéia F, Gusmão L A P, Hall Barbosa C R, Costa Monteiro E, Gonçalves L A P and Machado F L A (2008) Ring shaped magnetic field transducer based on the GMI effect. Meas. Sci. Technol. 19: 025801

[48] Phan M H , Peng H X (2008) Giant magnetoimpedance materials: Fundamentals and applications. Progress in Materials Science. 53: 323–420

[49] Squire PT, Atkinson D, Gibbs M R J, Atalay S J (1994) Amorphous wires and their applications. J Magn MagnMater. 132: 10–21

[50] Ohnaka I, Fukusako T, Matui T (1981) Preparation of amorphous wires. J. Jpn. Inst. Met. 45: 751–62.

[51] http://www.aichi-steel.co.jp/ENGLISH/pro_info/pro_intro/elect_3.html

[52] Panina L V, Mohri K, Uchiyama T, Noda M (1995) Giant magneto-impedance in Co-rich amorphous wires and films. IEEE Trans Magn. 31:1249–60

[53] Phan MH, Peng HX, Yu SC, Vazquez M (2006) Optimized giant magnetoimpedance effect in amorphous and nanocrystalline materials. J Appl Phys. 99: 08C505

[54] Sukstanskii A L and Korenivski V (2001) Impedance and surface impedance of ferromagnetic multilayers: the role of exchange interaction J. Phys. D 34: 3337

[55] Li B, Kosel J (2001) 3d Simulation of GMI Effect In Thin Film Based Sensors. J. Appl. Phys. 109: 07E519

[56] Dong C, Chen S, Hsu T Y (Xu Zuyao) (2003) A modified model of GMI effect in amorphous films with transverse magnetic anisotropy. J. Magn. Magn. Mater. 263: 78-82

[57] Xiao S, Liu Y, Dai Y, Zhang L, Zhou S, and Liu G (1999) Giant Magnetoimpedance Effect in Sandwiched Films. J. Appl. Phys. 85: 4127

[58] Xiao S, Liu Y, Yan S, Dai Y, Zhang L, and Mei L (2000) Giant Magnetoimpedance and Domain Structure in FeCuNbSiB Films and Sandwiched Films. Phys. Rev. B 61: 5734–5739

[59] de Cos D, Panina L V, Fry N, Orue I, Garcia-Arribas A, Barandiaran J M (2005) Magnetoimpedance in narrow NiFe/Au/NiFe multilayer film systems. IEEE Transactions on Magnetic. 41: 3697 - 3699

[60] Li X, Yuan W, Zhao Z, Ruan J and Yang X (2005) The GMI effect in Nanocrystalline FeCuNbSiB Multilayered Films with a SiO2 Outer Layer. J. Phys. D: Appl. Phys. 38: 1351–1354

[61] Corrêa M A, Bohn F, Escobar V M, Marques M S, Viegas A D C, Schelp L F, and Sommer R L (2011) Wide Frequency Range Magnetoimpedance in Tri-layered Thin NiFe/Ag/NiFe Films: Experiment and Numerical Calculation. J. Appl. Phys. 110: 093914

[62] Zhou Z, Zhou Y, Chen L and Lei C (2011) Transverse, Longitudinal and Perpendicular Giant Magnetoimpedance Effects in a Compact Multiturn Meander NiFe/Cu/NiFe Trilayer Film Sensor. Meas. Sci. Technol. 22: 035202

[63] Tobolka G (1979) Mixed matrix representation of SAW transducers. IEEE Trans. Sonics Ultrason. SU-26

[64] http://www.medicalelectronicsdesign.com/products/nanopower-magnetic-sensors-fit-implantable-devices

[65] Corchero J L, Villaverde A (2009) Biomedical Applications of Distally Controlled Magnetic Nanoparticles. Trends in Biotechnology 27: 468-476

[66] Ripka P (2008) Sensors based on bulk soft magnetic materials: Advances and challenges. Journal of Magnetism and Magnetic Materials. 320: 2466-2473

[67] Lenz J, Edelstein S (2006) Magnetic sensors and their applications. IEEE Sensors Journal. 6: 631-649

[68] Nishibe Y, Ohta N, Tsukada K, Yamadera H, Nonomura Y, Mohri K, Uchiyama T (2004) Sensing of passing vehicles using a lane marker on a road with built-in thin-film MI sensor and power source. IEEE Transactions on Vehicular Technology. 53: 1827- 1834

[69] Steindi R, Hausleitner C, Hauser H, Bulst W (2000) "Wireless magnetic field sensor employing SAW-transponder," Applications of Ferroelectrics. Proceedings of the 2000 12th IEEE International Symposium on. 2: 855-858

[70] Gloria N B S, Areiza M C L, Miranda I V J, Rebello J M A (2009) Development Of A Magnetic Sensor for Detection And Sizing of Internal Pipeline Corrosion Defects, NDT & E International. 42: 669-677

IntechOpen